Thermal and disorder fluctuations in anisotropic superconducting $Nd_{1.85}Ce_{0.15}CuO_{4-x}$ epitaxial films

N.-C. Yeh, W. Jiang, and D. S. Reed
Department of Physics, California Institute of Technology, Pasadena, California 91125

A. Gupta and F. Holtzberg
IBM Research Division, Thomas J. Watson Research Center, Yorktown Heights, New York 10598

A. Kussmaul
Francis Bitter National Magnet Laboratory, Massachusetts Institute of Technology, Cambridge, Massachusetts 02139

(Received 12 August 1991)

The anisotropic vortex transport properties of c-axis-oriented $Nd_{1.85}Ce_{0.15}CuO_{4-x}$ superconducting epitaxial films are found consistent with a dislocation-mediated second-order vortex-solid melting transition. The anisotropic critical exponents and the electronic mass ratio are determined from the scaling of the current-voltage characteristics. The nucleation energy of vortex dislocations due to both thermal and disorder fluctuations and its relation to the vortex elastic moduli is inferred from our experiments.

One of the most interesting issues facing high-temperature superconductors (HTS's) is the strongly fluctuation-influenced vortex states and vortex transport properties.[1-10] Both thermal and disorder fluctuations in HTS systems are crucial to the vortex dynamics and dissipation[1-8] because of the short superconducting coherence lengths and high transition temperatures. Although measurements of the vortex transport properties[9-12] appear dependent on the sample's defect structure, there is consistent experimental evidence[9-11] for a second-order vortex-solid melting transition in homogeneous HTS's. This raises two important questions: What is the mechanism of melting? How does the interplay of thermal and disorder fluctuations influence the nature of the melting transition? One proposed mechanism is the vortex screw and edge-dislocation-driven melting.[1,2] In this Brief Report we offer transport evidence for this mechanism from our studies of the electron-doped superconducting oxide $Nd_{1.85}Ce_{0.15}CuO_{4-x}$ (Nd-Ce-Cu-O) c-axis-oriented epitaxial films, which we compare to the results of $YBa_2Cu_3O_7$ (Y-Ba-Cu-O) single crystals and epitaxial films.

The electron-doped superconductors $L_{1.85}M_{0.15}CuO_{4-x}$ (L = Pr, Nd, Sm, Eu, and Gd; M = Ce and Th) differ from the hole-doped superconductors (e.g., Y-Ba-Cu-O) in various interesting ways: (1) The superconducting transition temperatures in the former are generally much lower than those of the latter,[13] with a maximal $T_c \approx 23$ K for $Nd_{1.85}Ce_{0.15}CuO_4$, compared with $T_c \approx 93$ K for $YBa_2Cu_3O_7$. Consequently, vortex thermal fluctuations in the electron-doped superconducting oxides are suppressed, and disorder fluctuations become more important. (2) Hole-doped HTS's have a highly stressed orthorhombic structure, causing a high density of large defects (such as twin and grain boundaries) in the epitaxial film growth, which are greatly reduced by the more stable tetragonal structure of electron-doped HTS's.[13] (3) The M cations in the $L_{1.85}M_{0.15}CuO_{4-x}$ system distribute randomly over the L sites, thereby forming "intrinsic disorder" in these superconducting oxides. We show in the following that disorder fluctuations in high-quality $Nd_{1.85}Ce_{0.15}CuO_{4-x}$ epitaxial films play an important role in determining the critical phenomena near the vortex-solid melting transition and that the melting transition is driven by flux-line dislocations, with the nucleation energy of dislocations determined by the elastic moduli of the vortex solid.

Two length scales (the correlation length ξ and characteristic time τ) determine the physical properties near a second-order phase transition. Typically, we define $\xi \approx \xi_0 |1-(T/T_c)|^{-\nu}$ and $\tau \sim \xi^z$, where ν and z are the static and dynamic exponents, respectively, ξ_0 is the zero-temperature correlation length, and T_c is the critical temperature. In an anisotropic superconductor with a uniaxial symmetry, there are two independent static exponents ($\nu_\parallel$ and $\nu_\perp$) and critical temperatures [$T_M(H_\parallel)$

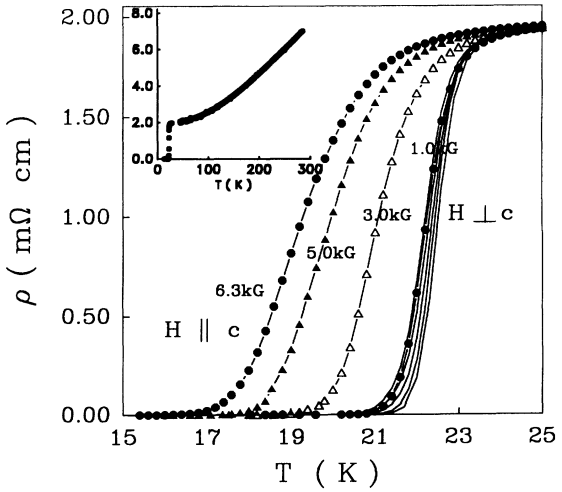

FIG. 1. Resistivity (ρ) vs temperature (T) data of $Nd_{1.85}Ce_{0.15}CuO_4$. Dotted lines, $\mathbf{H} \| c$ axis; solid lines, $\mathbf{H} \perp c$ axis at $H = 0$, 1.0, 3.0, 5.0, and 6.3 kG. The resistivity shown here is obtained from $\rho = E/J$, with $J = 0.2$ A/cm^2, and the Ohmic behavior $E \propto J$ is obeyed for the data shown. The inset shows the resistivity data up to 300 K with the y axis in units of mΩ cm.

and $T_M(H_\perp)$] for the two independent magnetic-field (H) orientations $\mathbf{H}\|c$ and $\mathbf{H}\perp c$. Following Refs. 6 and 9, the scaling relation between the electric field (E) and applied current density (J) near the vortex-solid melting transition temperature $T_M(H)$ is (for a given magnetic field along a principal axis)

$$E(J,T)\sim J\rho(J,H,T)\propto J\xi^{d-2-z}\tilde{E}_{\pm}(x)\ ,$$
$$x\equiv J\Phi_0\xi^{d-1}/(k_BT)\ , \tag{1}$$

where ρ is the resistivity, Φ_0 is the flux quantum, $\xi\approx\xi_0|1-(T/T_M)|^{-\nu}$, d is the dimensionality, and $\tilde{E}_{\pm}(x)$ are universal functions:[6] $\tilde{E}_+(x)\approx\tilde{E}_-(x)\sim x^{(z+2-d)/(d-1)}$ as $x\to\infty$, so that $E(J)\propto J^{(z+1)/(d-1)}$ at T_M; $\tilde{E}_-(x)\propto\exp[-(x_0/x)^\mu]$ and $\tilde{E}_+(x)\to$const as $x\to 0$. (x_0 is a constant independent of T and J.) Assuming that the universal function $\tilde{E}_-(x)$ below $T_M(H)$ is governed by the nucleation rate of flux-line dislocations in the presence of external currents,[6,9] the dislocation nucleation energy $U(T,H,J)$ is related to $\tilde{E}_-$ by the scaling relation [see Eq. (1)]

$$\tilde{E}_-(x)=a\exp\left[-\frac{U(x)}{k_BT}\right]\ ,$$
$$\frac{U(x)}{k_BT}=\frac{U(T,H,J)}{k_BT}=b\left[\frac{|1-T/T_M(H)|^{(d-1)\nu}(k_BT)}{(J\xi_0^{d-1})\Phi_0}\right]^\mu\ , \tag{2}$$

where a and b are coefficients independent of T and J, k_B is the Boltzmann constant, and ξ_0 is a function of H. Thus the dislocation nucleation energy $U(T,H,J)$ can be determined directly from the experimental E-J curves at $T<T_M(H)$. We note that the melting temperatures $T=T_M(H)$ on the H-T phase diagram satisfies the relation $H_M(T)=H_M(0)[1-(T/T_{c0})]^{2\nu_0}$, where T_{c0} is the zero-field superconducting transition temperature and ν_0 is the critical exponent associated with the multicritical point T_{c0}. In the mean-field approximation, $\nu_0=\frac{1}{2}$.

Before proceeding to the experimental results and analysis of Nd-Ce-Cu-O epitaxial films, we address an important issue regarding how $U(T,H,J)$ may be related to the elastic properties of the vortex solid. We note that the product $J\xi^{d-1}$ can be generalized as $J\xi_l\xi_t^{d-2}$, where ξ_l and ξ_t are the longitudinal and transverse vortex correlation lengths, respectively. Both ξ_l and ξ_t have the same critical exponents (ν and z) and critical temperature $T_M(H)$ for a given magnetic-field direction. For $d=3$ and in the absence of strong disorder, the longitudinal and transverse vortex correlation lengths can be expressed in terms of the sheer (C_{66}) and tilt (C_{44}) elastic moduli[1,8]:

$$\xi_l\approx\frac{2\pi k_BTH}{\sqrt{3}\Phi_0C_{66}}\ ,\quad \xi_t\approx\frac{2\pi k_BTH}{\sqrt{3}\Phi_0\sqrt{C_{66}C_{44}}}\ . \tag{3}$$

Thus the nucleation energy of vortex dislocations can be

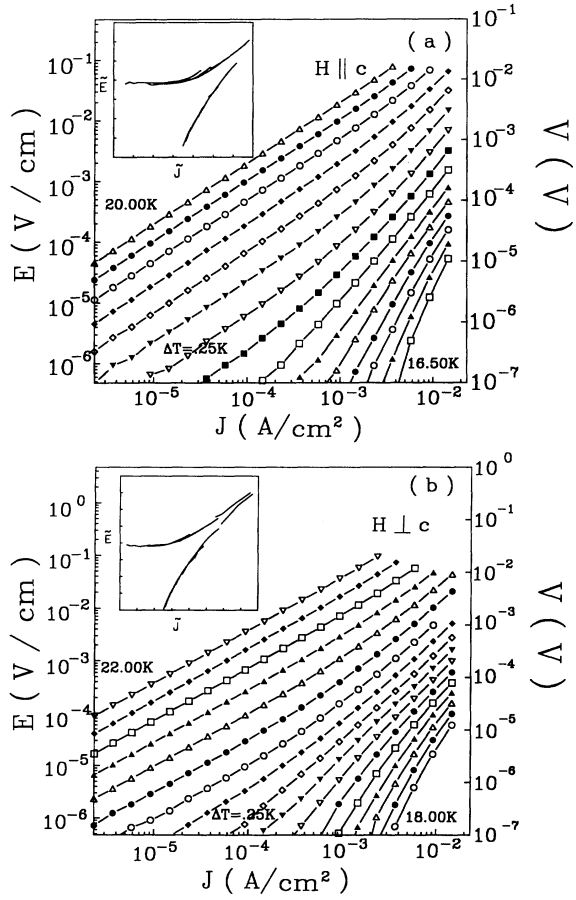

FIG. 2. Isothermal electric-field (E) vs current-density (J) curves of Nd-Ca-Cu-O for $H=3$ kOe and (a) $\mathbf{H}\|c$ axis; (b) $\mathbf{H}\perp c$ axis. The temperatures are 0.25 K apart unless specified. The insets show the log-log plot of universal functions obtained from collapsing the isothermal E-vs-J curves at $H=3.0$ kOe. [The collapsed universal functions are the same for $H=1.0$, 2.0, 4.0, 5.0, and 6.3 kOe, and $\tilde{J}\equiv J|1-(T/T_M)|^{-2\nu}$.] (a) $\mathbf{H}\|c$ axis, with parameters $\nu_\|=2.1\pm0.1$ and $z_\|=3.0\pm0.1$ ($\tilde{E}=10^0\to10^7$, $\tilde{J}=10^{-2}\to10^5$); (b) $\mathbf{H}\perp c$ axis, with parameters $\nu_\perp=2.7\pm0.2$ and $z_\perp=2.5\pm0.1$ ($\tilde{E}=10^0\to10^8$, $\tilde{J}=10^{-1}\to10^7$). From $\tilde{E}_-(x)\sim\exp[-(J_0/J)^\mu]$, we obtain $\mu=0.10\pm0.01$ for all magnetic fields.

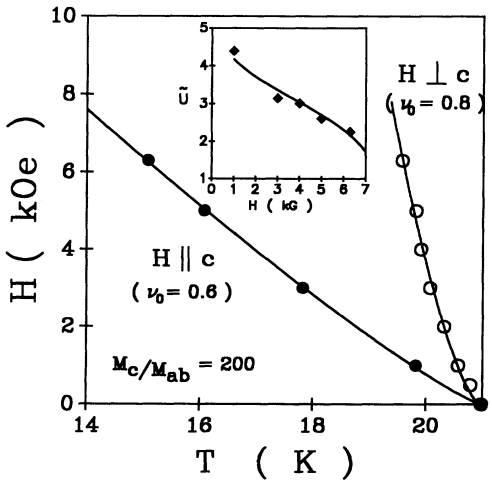

FIG. 3. Melting transition lines for $\mathbf{H}\perp c$ and $\mathbf{H}\|c$ on the H-T vortex phase diagram. The mass anisotropy ratio thus determined is $(M_c/M_{ab})\sim200$. The inset shows scaling of the nucleation energies for both $\mathbf{H}\perp c$ and $\mathbf{H}\|c$. The scaling function $\tilde{U}$ (solid line) using Eq. (6) and $\mu\approx0.1$ are in excellent agreement with the experimental results (points).

obtained from Eqs. (2) and (3):

$$\frac{U(T,H,J)}{k_BT} \propto \left[\frac{C_{66}^{3/2}C_{44}^{1/2}}{J(k_BT)H^2}\right]^{\mu} \sim \left[\frac{(k_BT)|1-[T/T_M(H)]|^{2\nu}}{J}\right]^{\mu} . \quad (4)$$

Note that both C_{66} and C_{44} depend on T and H (Refs. 3, 4, and 14) and that $U=0$ at $T=T_M$.

To obtain a direct comparison of Eq. (4) to existing mean-field elastic theory, the following mean-field approximations for C_{66} and C_{44} are assumed[3,4,14]:

$$C_{44} \propto H^2[1-(T/T_{c0})] , \quad C_{66} \propto H_M(T)^2(1-h)^2 , \quad (5)$$

where $h \equiv H/H_M(0)$. From Eqs. (4) and (5) and $H_M(T)=H_M(0)|1-(T/T_{c0})|^{2\nu_0}$, we obtain

$$\frac{U}{k_BT} \sim \frac{|1-(T/T_{c0})|^{\mu/2}}{(HTJ)^{\mu}}\left[\left[1-\frac{T}{T_{c0}}\right]^{2\nu_0}-\frac{H}{H_M(0)}\right]^{3\mu} . \quad (6)$$

Since values of $T_M(H)$, T_{c0}, ν, and μ are obtained directly from the scaling analysis of E-J curves [see Eq. (1)], the exponent ν_0 is determined by the relation in Eq. (6), which can be compared to that of the melting line $H_M(T)=H_M(0)|1-(T/T_{c0})|^{2\nu_0}$, for consistency. However, we note that the comparison of Eq. (4) to Eq. (6) is valid only if $H \ll H_M(0)$. In the high-field limit and for $|T_M(H)-T| \ll |T_{c0}-T|$, the mean-field expressions for C_{66} and C_{44} in Eq. (5) are no longer rigorous and should be renormalized to satisfy Eq. (4). A theory of such renormalizations is still to be developed.

The well-characterized [using x-ray diffraction, scanning electron microscopy (SEM), Rutherford backscattering spectroscopy (RBS), and x-ray photoemission spectroscopy (XPS)] single-phased samples in this work include one $Nd_{1.85}Ce_{0.15}CuO_4$ epitaxial film (1800 Å thick) on $SrTiO_3$ substrates, as well as one $YBa_2Cu_3O_7$ single crystal and one $YBa_2Cu_3O_7$ epitaxial film on $SrTiO_3$ for comparison. The sample preparations and characterizations of Nd-Ce-Cu-O laser-ablated epitaxial films have been described in Ref. 15. Details of the Y-Ba-Cu-O sample characterizations, electrical contact fabrications, and the transport measurement techniques are given elsewhere.[9] Figure 1 shows the Ohmic resistivity versus temperature data for $\mathbf{J}\perp\mathbf{H}$ with $\mathbf{H}\|c$, and, for $\mathbf{J}$, $\mathbf{H}$, and c mutually perpendicular, at various magnetic fields. Note that for $\mathbf{H}\|c$, the resistivity broadens more than that for $\mathbf{H}\perp c$. The inset shows the resistivity data up to room temperature. Figure 2 shows the isothermal E-J curves for $\mathbf{H}\|c$ and $\mathbf{H}\perp c$. (The E-J measurements were performed at $H=0$, 1, 2, 3, 4, 5, and 6.3 kOe. Only the 3-kOe data are shown.) Well above the melting temperature $T_M(H)$ [the "melting temperatures" $T_M(H)$ are defined below from scaling analysis], the E-J isothermal curves are Ohmic. As the temperature approaches $T_M(H)$ from above, the E-J curves begin to depart from the Ohmic behavior at higher current densities. A sharp nonlinear behavior develops at $T<T_M(H)$. Similar behavior is observed for both magnetic-field directions.

Applying Eq. (1) to the Nd-Ce-Cu-O data in Fig. 2, we can collapse all E-J curves into the universal functions $\tilde{E}_{\pm}$ (insets of Fig. 2) by plotting $[(E/J)|1-(T/T_M)|^{\nu(d-2-z)}]$ vs $[J|1-(T/T_M)|^{\nu(1-d)}]$ [see Eq. (1)]. Assuming $d=3$, we obtain $\nu_{\|}=2.1\pm0.1$,

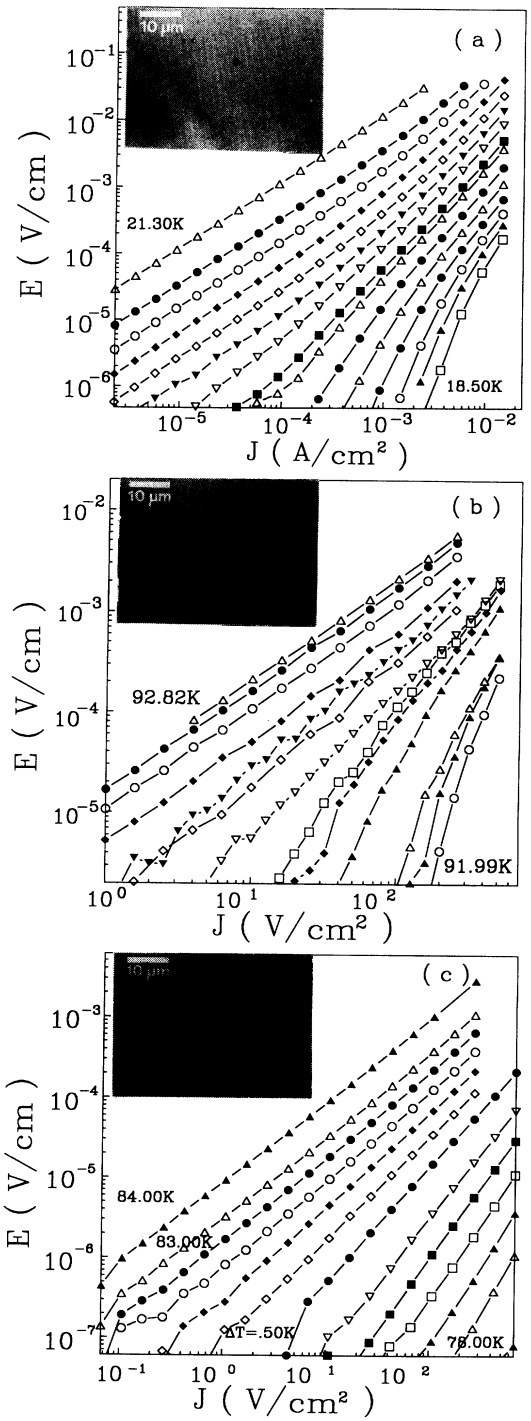

FIG. 4. E-J isothermal curves at $H=1$ kOe and the corresponding SEM photographs of (a) a Nd-Ca-Cu-O epitaxial film on $SrTiO_3$, (b) a Y-Ba-Cu-O single crystal, and (c) a Y-Ba-Cu-O epitaxial film on $SrTiO_3$. The E-J curves of (a) and (b) show clear evidence of a phase transition. On the other hand, the E-J curves of sample (c), which has a high density of structural defects, are consistent with the Ambegaokar-Halperin model (Refs. 9 and 20).

$z_{\parallel}=3.0\pm0.1$, $\nu_{\perp}=2.7\pm0.2$, $z_{\perp}=2.5\pm0.1$, and $\mu=0.10\pm0.01$ for both $\mathbf{H}\|c$ and $\mathbf{H}\perp c$. The $T_M(H)$ values determined from collapsing the E-J isothermal curves are shown in Fig. 3. Note that the same exponents $(\nu_{\parallel},z_{\parallel})$, $(\nu_{\perp},z_{\perp})$, and μ have been used for the E-J curves in all fields, confirming an important fact that the melting transitions for a given field direction on the $T_M(H)$ line belong to the same universality class. Also note that $\nu_{\parallel}z_{\parallel}\approx\nu_{\perp}z_{\perp}$, indicating universal critical dynamics $(\tau\sim\xi^{z}\sim|1-T/T_M|^{-\nu z})$ for both $\mathbf{H}\|c$ and $\mathbf{H}\perp c$. The fact that μ is considerably smaller than 1 implies a large vortex anisotropy and a significant degree of disorder.[6,9] In Fig. 3 the anisotropic melting transition lines satisfy the relations $H_{M\parallel}(T)=H_{M\parallel}(0)|1-(T/T_{c0})|^{2\nu_{0\parallel}}$ and $H_{M\perp}(T)=H_{M\perp}(0)|1-(T/T_{c0})|^{2\nu_{0\perp}}$, with the critical exponents $\nu_{0\parallel}\approx0.6$, $\nu_{0\perp}\approx0.8$, $H_{M\parallel}(0)\approx30$ kOe, and $H_{M\perp}(0)\approx400$ kOe. The effective-mass ratio determined from the relation $\Gamma^2\equiv(M_c/M_{ab})=[H_{M\perp}(0)/H_{M\parallel}(0)]^2$ gives $\Gamma^2\approx180$. We note that the ratio obtained here is determined by scaling theory. For comparison, the mass ratio (M_c/M_{ab}) previously estimated for Nd-Ce-Cu-O $(\Gamma^2\approx420)$ and Sm-Th-Cu-O $(\Gamma^2\approx29)$ systems[16,17] were obtained by assigning the 50% resistive transition temperature in a constant magnetic field as a point on the $H_M(T)$ line.

The inset of Fig. 3 shows the magnetic scaling of the nucleation energies for both $\mathbf{H}\|c$ and $\mathbf{H}\perp c$. As shown by the theoretical curve

$$\tilde{U}=c_1\left[\frac{|1-(T/T_{c0})|^{\mu/2}}{H^{\mu}}\right]\left[\left[1-\frac{T}{T_{c0}}\right]^{2\nu_0}-\frac{H}{H_M(0)}\right]^{3\mu}$$

(solid line), the experimental data $\tilde{U}\equiv(U/T)(JT)^{\mu}$ at $T=19.0$ K (points) satisfy the relation in Eq. (6). (c_1 is a constant, which is the only adjustable parameter and is independent of T, H, and J.) Furthermore, using the temperature scaling in Eq. (6) and the parameters $\nu_{\parallel}$, $\nu_{\perp}$, μ, and $T_M(H)$ determined by collapsing the E-J isothermal curves for a given H, we again find the exponents $\nu_{0\parallel}\approx0.6$ and $\nu_{0\perp}\approx0.9$, in excellent agreement with those obtained from directly plotting $H_M(T)$. The same analysis applied to Y-Ba-Cu-O single crystals yields $\nu_{0\parallel}\approx0.7$, consistent with the experimental value.[9]

In Fig. 4 the strong correlation between the vortex transport properties and sample homogeneity is manifested by the E-J isothermal curves at $H=1$ kOe and the SEM photographs of various HTS samples: (a) a Nd-Ce-Cu-O epitaxial film, (b) a Y-Ba-Cu-O single crystal, and (c) a Y-Ba-Cu-O epitaxial film. We note that both the Nd-Ce-Cu-O epitaxial film and Y-Ba-Cu-O single crystal are very homogeneous, and the E-J characteristics of both systems show clear evidence of a phase transition. The key difference between (a) and (b) is the relatively larger critical exponents of Nd-Ce-Cu-O ($\nu_{\parallel}\approx2.1$, $\nu_{\perp}\approx2.7$, $z_{\parallel}\approx3.0$, $z_{\perp}\approx2.5$), compared to those of Y-Ba-Cu-O ($\nu_{\parallel}=0.9\pm0.2$, $z_{\parallel}=2.0\pm0.2$).[9] This difference may be attributed to the presence of intrinsic disorder (Ce) in Nd-Ce-Cu-O and to the more dominant role of disorder fluctuations in Nd-Ce-Cu-O due to smaller thermal fluctuations. We also note an interesting contrast between samples (a) and (c): The gradual change in the E-J isothermal curves of the Y-Ba-Cu-O film implies the absence of a well-defined phase transition. The SEM photograph (c) also shows a high density of large scale defects due to the screw dislocations during the film-growth process.[18,19] These "extrinsic" defects may be responsible for the Ambegaokar-Halperin weak-link behavior[20] in the E-J characteristics.[9] From Fig. 4 it is obvious that the vortex transport properties are extremely sensitive to the defect structure of a superconductor. However, direct calculations of the vortex phase-transition temperatures and critical exponents by incorporating thermal and disorder fluctuations remain a theoretical challenge.

In summary, the anisotropic vortex transport properties of the electron-doped high-temperature superconductor $Nd_{1.85}Ce_{0.15}CuO_4$ are found to be consistent with a second-order vortex-solid melting transition. The larger static and dynamic critical exponents of the Nd-Ca-Cu-O system ($\nu_{\parallel}\approx2.1$, $\nu_{\perp}\approx2.7$, $z_{\parallel}\approx3.0$, $z_{\perp}\approx2.5$) are suggestive of a more disordered vortex structure, in contrast to the finding in $YBa_2Cu_3O_7$ single crystals.[9] By connecting the nucleation energy of dislocations to the elastic moduli of the vortex solid, we have provided experimental evidence for a dislocation-mediated melting transition.

We thank Nils Asplund for technical assistance and Professor M. C. Cross for helpful discussions. This work is jointly supported by NASA/OAET, ONR Grant No. N00014-91-J-1556 Caltech, JPL, IBM, and the consortium for Superconducting Electronics (DARPA Grant No. MDA972-90-C-0021). One of us (N.-C. Y.) gratefully acknowledges support by the Alfred P. Sloan Foundation.

[1]D. R. Nelson and P. Le Doussal, Phys. Rev. B **42**, 10 113 (1990); D. R. Nelson and H. S. Seung, *ibid.* **39**, 9153 (1989).
[2]M. C. Marchetti and D. R. Nelson, Phys. Rev. B **41**, 1910 (1990).
[3]A. Sudbø and E. H. Brandt, Phys. Rev. Lett. **66**, 1781 (1991); Phys. Rev. B **43**, 10 482 (1990).
[4]E. H. Brandt, Phys. Rev. Lett. **63**, 1106 (1989).
[5]A. Houghton *et al.*, Phys. Rev. B **40**, 6763 (1989).
[6]D. S. Fisher *et al.*, Phys. Rev. B **43**, 130 (1991).
[7]M. P. A. Fisher, Phys. Rev. Lett. **62**, 1415 (1988).
[8]N-C. Yeh, Phys. Rev. B **42**, 4850 (1990).
[9]N.-C. Yeh *et al.*, Phys. Rev. B **45**, 5654 (1992).
[10]T. K. Worthington *et al.*, Cryogenics **30**, 417 (1990).
[11]P. L. Gammel *et al.*, Phys. Rev. Lett. **66**, 953 (1991).
[12]R. Koch *et al.*, Phys. Rev. Lett. **63**, 1511 (1989).
[13]Y. Tokura *et al.*, Nature **337**, 345 (1989).
[14]E. H. Brandt, J. Low Temp. Phys. **26**, 709 (1977); **26**, 735 (1977); **28**, 263 (1977); **28**, 291 (1977).
[15]A. Gupta *et al.*, Appl. Phys. Lett. **55**, 1795 (1989).
[16]Y. Dalichaouch *et al.*, Phys. Rev. Lett. **64**, 599 (1990).
[17]Y. Hidaka and M. Suzuki, Nature **338**, 635 (1989).
[18]Ch. Gerber *et al.*, Nature **350**, 279 (1991).
[19]M. Hawley *et al.*, Science **251**, 1587 (1991).
[20]V. Ambegaokar and B. I. Halperin, Phys. Rev. Lett. **22**, 1364 (1969).

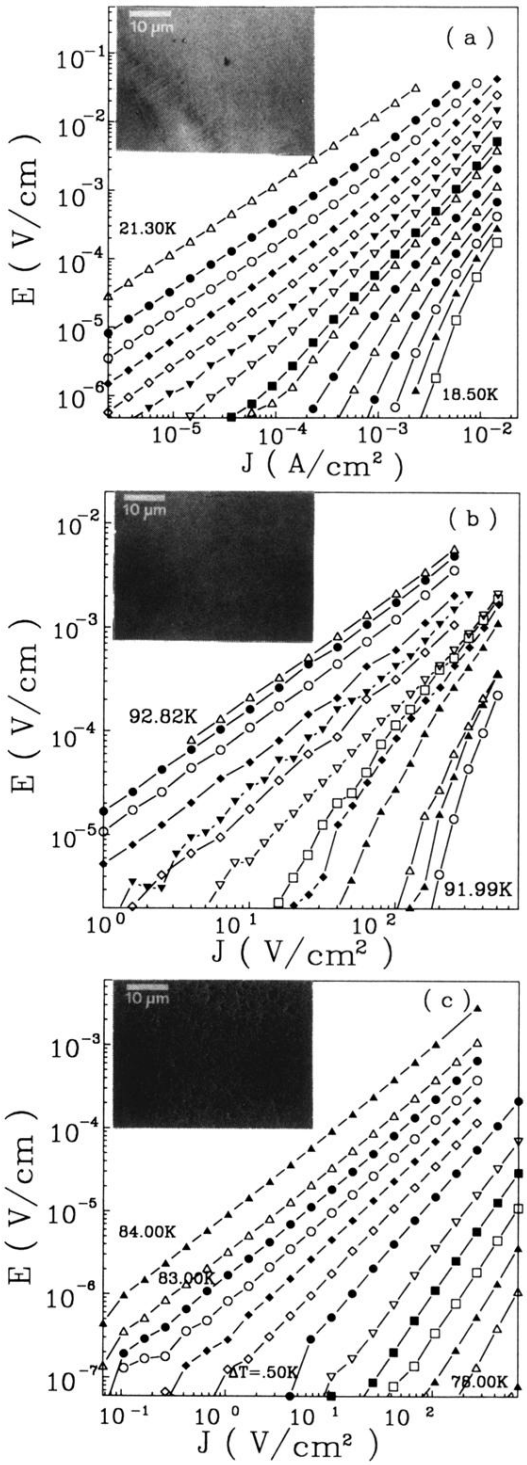

FIG. 4. *E-J* isothermal curves at $H = 1$ kOe and the corresponding SEM photographs of (a) a Nd-Ca-Cu-O epitaxial film on $SrTiO_3$, (b) a Y-Ba-Cu-O single crystal, and (c) a Y-Ba-Cu-O epitaxial film on $SrTiO_3$. The *E-J* curves of (a) and (b) show clear evidence of a phase transition. On the other hand, the *E-J* curves of sample (c), which has a high density of structural defects, are consistent with the Ambegaokar-Halperin model (Refs. 9 and 20).